

# Macroscopic Alignment and Assembly of $\pi$ -Conjugated Oligopeptides Using Colloidal Microchannels

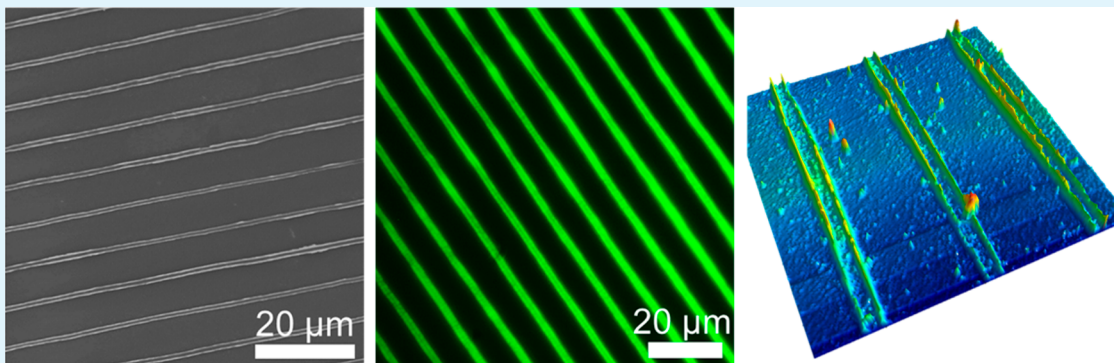
Bo Li,<sup>†</sup> Lawrence R. Valverde,<sup>‡</sup> Fengjiao Zhang,<sup>†</sup> Yuecheng Zhou,<sup>‡</sup> Songsong Li,<sup>‡</sup> Ying Diao,<sup>†</sup><sup>ID</sup> William L. Wilson,<sup>\*,†,§,||</sup> and Charles M. Schroeder<sup>\*,†,‡,§,||</sup>

<sup>†</sup>Department of Chemical and Biomolecular Engineering and <sup>§</sup>Frederick Seitz Materials Research Laboratory, University of Illinois at Urbana–Champaign, Urbana, Illinois 61801, United States

<sup>‡</sup>Department of Materials Science and Engineering, University of Illinois at Urbana–Champaign, Urbana, Illinois 61820, United States

<sup>||</sup>Center for Nanoscale Systems Faculty of Arts and Sciences, Harvard University, Cambridge, Massachusetts 02138, United States

## Supporting Information



**ABSTRACT:** One-dimensional (1-D) supramolecular self-assembly offers a powerful strategy to achieve long-range unidirectional ordering of organic semiconducting materials via noncovalent interactions. Using a hierarchical assembly, electronic and optoelectronic materials can be constructed for applications including organic conducting nanowires, organic field-effect transistors (OFETs), and organic light-emitting devices (OLEDs). Despite recent progress, it remains challenging to precisely align and assemble 1-D structures over large areas in a rapid and straightforward manner. In this work, we demonstrate a facile strategy to macroscopically align supramolecular fibers using a templating method based on sacrificial colloidal microchannels. Through use of this approach, colloidal microchannels are generated on a solid surface using a simple fabrication method, followed by the spontaneous self-assembly of  $\pi$ -conjugated oligopeptides inside large arrays of microchannels triggered by solvent evaporation. Following oligopeptide assembly and removal of sacrificial microchannels, the structural properties of oligopeptide fibers were characterized using atomic force microscopy (AFM), atomic force microscope–infrared spectroscopy (AFM–IR), photoinduced force microscopy (PiFM), fluorescence polarization microscopy, and electron microscopy. These results reveal the macroscopic alignment of oligopeptide fibers into ordered structures over millimeter length scales, facilitated by colloidal microchannel templating. In addition, the charge transport properties ( $I$ – $V$  curves) of  $\pi$ -conjugated oligopeptides assembled using this method were determined under a wide range of applied voltages using interdigitated array electrodes and conductive AFM. Overall, this work illustrates a simple yet robust strategy to pattern 1-D supramolecular fibers over large areas, thereby offering new routes for assembling materials for organic electronics.

**KEYWORDS:**  $\pi$ -conjugated oligopeptides, colloidal microchannels, self-assembly, atomic force microscope–infrared spectroscopy (AFM–IR), photoinduced force microscopy (PiFM)

## INTRODUCTION

Charge transport in organic semiconducting materials has enabled the development of several emerging technologies such as next-generation solar cells and plastic transistors.<sup>1</sup> Modest control over electronic delocalization in soft semiconducting materials can be achieved by local ordering of conductive molecular subunits and  $\pi$ – $\pi$  stacking interactions during supramolecular assembly. However, device performance is

ultimately determined by electronic interactions occurring across multiple length scales within self-assembled structures in organic semiconductors. In particular, the specific chemical features underlying long coherence length structures ultimately

**Received:** September 14, 2017

**Accepted:** November 7, 2017

**Published:** November 7, 2017

define the emergent electronic properties of these materials. Despite recent progress, the fundamental mechanisms determining device performance in molecular electronics are not fully understood due to the inability to completely control molecular interactions during self-assembly.<sup>2</sup>

One-dimensional (1-D) supramolecular self-assembly offers a powerful strategy to achieve long-range unidirectional ordering of organic semiconducting subunits via noncovalent interactions. Development of 1-D assembled materials has enabled applications in organic conducting nanowires,<sup>3</sup> organic field-effect transistors (OFETs),<sup>4,5</sup> and organic light-emitting devices (OLEDs).<sup>6</sup> Despite recent progress, a key challenge hindering the ongoing development and application of these materials lies in the ability to precisely align 1-D nanomaterials in desired orientations using simple and straightforward methods.<sup>7</sup> For example, carbon nanotubes were identified as ideal candidates for next-generation transistors due to high charge mobility and thermal conductivity,<sup>8,9</sup> however, facile alignment of carbon nanotubes into ordered structures over large areas required nearly a decade of work.<sup>10–14</sup> In addition, self-assembly of thiophene-based conjugated polymers for electronic applications have also been widely investigated.<sup>15–17</sup> From this perspective, the alignment of assembled supramolecular fibers into well-ordered arrays remains an important albeit challenging task in the field.

Synthetic  $\pi$ -conjugated oligopeptides are known to spontaneously self-assemble into ordered 1-D supramolecular structures due to high levels of directional hydrogen bonding and  $\pi$ – $\pi$  stacking interactions.<sup>18</sup> For  $\pi$ -conjugated oligopeptides rich in acidic residues (e.g., aspartic acid, glutamic acid), self-assembly can be triggered by lowering solution pH via acid vapor diffusion or direct addition of acid to an aqueous solution of peptide.<sup>19–21</sup> Recently, Li et al. demonstrated an organic liquid interfacial isolation strategy to control the kinetics of assembly by regulating the rate of acid diffusion, thereby yielding homogeneous solutions of self-assembled  $\pi$ -conjugated oligopeptides.<sup>22</sup> In an alternative approach, the rate of oligopeptide self-assembly was controlled using an acid-generating chemical reaction based on hydrolysis of glucono- $\delta$ -lactone.<sup>23</sup> Nevertheless, these prior methods generally result in aqueous gels consisting of  $\pi$ -conjugated oligopeptide fibers in random orientations, materials that are notoriously difficult to align postassembly.

Recent work has shown that  $\pi$ -conjugated oligopeptides undergo a sol–gel transition upon increasing the concentration of oligopeptide in aqueous solution at neutral pH, which was characterized using a combination of microrheology and optical spectroscopy.<sup>24</sup> These results are consistent with the concentration-driven self-assembly of discotic molecules, which is thought to occur due to enthalpic effects including  $\pi$ – $\pi$  stacking interactions and hydrogen bonding.<sup>25</sup> In addition, peptide amphiphiles can also self-assemble due to hydrophobic interactions and hydrogen bonding.<sup>26</sup> From this perspective, we hypothesized that solvent evaporation could provide an alternative pathway to trigger self-assembly without the direct addition of acid by simply increasing oligopeptide concentration during solvent evaporation. To demonstrate this idea, we carried out evaporative self-assembly of  $\pi$ -conjugated oligopeptides inside sacrificial microchannel arrays patterned on a solid substrate.

In this work, we demonstrate a facile strategy to assemble and align supramolecular fibers over millimeter-sized length scales using colloidal microchannels. First, we studied the

evaporative assembly of  $\pi$ -conjugated oligopeptides into 1-D fibers on a solid substrate. Interestingly, we found that the helical structure of assembled peptide fibers is strongly dependent on the organic solvent used for evaporative assembly. We then directed the evaporative assembly of  $\pi$ -conjugated oligopeptides inside sacrificial colloidal microchannels on a solid substrate. Here, a simple fabrication strategy is used to generate macroscopic arrays of colloidal microchannels by drying a film of polystyrene latex nanoparticles on a solid substrate, which forms highly ordered microchannel features due to capillary stresses during film drying.<sup>27</sup> These sacrificial microchannels are then used to direct the assembly and alignment of supramolecular fibers of  $\pi$ -conjugated oligopeptides. Following selective removal of colloidal channels, highly ordered patterns of assembled oligopeptides are obtained on a solid surface over relatively large millimeter-sized length scales. Following assembly, we systematically investigated the structural and optical properties of oligopeptide fibers using a combination of fluorescence microscopy, atomic force microscopy (AFM)–infrared spectroscopy, known as AFM–IR, photoinduced force microscopy (PiFM), and electron microscopy. In addition, we studied the conductivity and electron transport properties of  $\pi$ -conjugated oligopeptide fibers using interdigitated array electrodes and conductive AFM. Taken together, our results show that evaporative assembly results in ordered arrays of aligned and electrically conductive oligopeptides over relatively large areas.

## EXPERIMENTAL METHODS

**Materials.** Sequence-defined synthetic oligopeptides with  $\pi$ -conjugated cores were synthesized using solid phase peptide synthesis (SPPS), as previously reported.<sup>28,29</sup>  $\pi$ -Conjugated oligopeptides containing a quaterthiophene (4T) core were flanked by symmetric peptides with a primary amino acid sequence Asp–Phe–Ala–Gly. The overall sequence of the  $\pi$ -conjugated oligopeptide is HO-DFAG-4T-GAFD-OH (abbreviated as DFAG-4T).

**Preparation of Colloidal Microchannels and DFAG-4T Patterns.** A polystyrene latex nanoparticle suspension (47 nm diameter particles) was purchased from Agilent Technologies (Batch 0006222658, 10.0% w/w particulate solids) and diluted at ratio of 1:9 into distilled, deionized (DI) water. A silicon (Si) wafer was cleaned by piranha solution (3:1 mixture of concentrated H<sub>2</sub>SO<sub>4</sub> and H<sub>2</sub>O<sub>2</sub>), followed by copious rinsing with DI water and drying with nitrogen. A small amount (60  $\mu$ L) of the diluted colloidal suspension was drop cast onto a clean Si wafer heated at 55 °C and allowed to dry for 20 min, yielding spoke-like colloidal microchannels.<sup>30</sup> The Si wafer containing the dry colloidal film was then thermally annealed at 105 °C for 30 min to remove structural defects in the film morphology, thereby generating a large array of colloidal microchannels. Following microchannel preparation, a small amount of DFAG-4T solution (10  $\mu$ L in organic solvent) was drop cast in the center of the Si wafer containing microchannels, thereby allowing the peptide solution to flow inside colloidal microchannels by capillary action. Following peptide deposition by evaporative assembly, the sacrificial colloidal microchannels were removed by soaking in toluene overnight for at least 24 h.

**Optical, Structural, And Electrical Characterization.** Assembled peptide morphologies were imaged using a Hitachi S4800 high-resolution Scanning Electron Microscope (SEM) and an Asylum Research MFP-3D Atomic Force Microscopy (AFM). Scanning probe spectral data are obtained using two systems. AFM–IR images and spectral data are obtained using a Neaspec neaSNOM, which is an apertureless system with pseudoheterodyne detection. A Daylight Systems MIRcat-QT Quantum Cascade Laser (QCL) serves as the tunable source. Photoinduced force hyperspectral images are obtained using a Molecular Vista VistaScope configured for hyperspectral imaging in the IR using a Block Engineering LaserTune Quantum

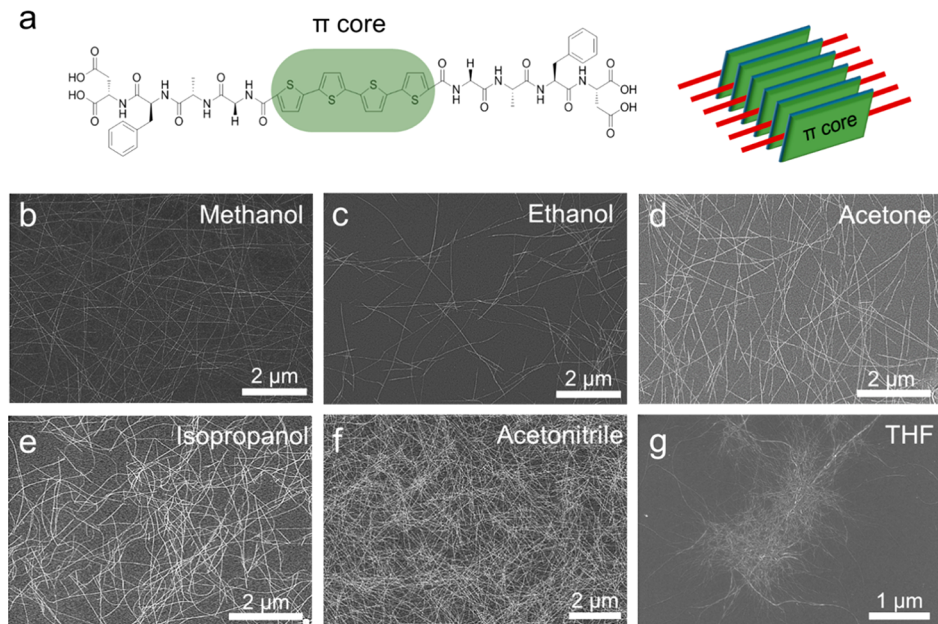


**Figure 1.** Evaporative self-assembly of  $\pi$ -conjugated oligopeptides. (a) Chemical structure of  $\pi$ -conjugated oligopeptide (DFAG-4T) and schematic illustration of 1-D self-assembly mediated by hydrogen bonding of peptide side chains and  $\pi$ - $\pi$  stacking interactions within aromatic cores. (b–g) Scanning electron microscopy (SEM) images of self-assembled DFAG-4T fibers formed by rapid evaporative self-assembly using a variety of organic solvents.

Cascade Laser (QCL). Conductive probe  $I$ – $V$  measurements were carried out with Keysight B1500A under a nitrogen atmosphere. Polarized fluorescence emission microscopy was performed on aligned DFAG-4T fibers using a Zeiss LSM710 inverted microscope in two-photon mode with a Ti:sapphire laser system (Mai-Tai, Spectra Physics) using an excitation wavelength of 780 nm. Interdigitated array (IDA) electrodes with a 2  $\mu\text{m}$  gap were purchased from ALS Co. (Catalog No. 012257).

## RESULTS AND DISCUSSION

We began by studying the self-assembly of  $\pi$ -conjugated oligopeptides containing a quaterthiophene (4T) core flanked by symmetric peptides with a primary amino acid sequence Asp–Phe–Ala–Gly. The overall sequence of the  $\pi$ -conjugated oligopeptide is HO-DFAG-4T-GAFD-OH (abbreviated as DFAG-4T), as shown in Figure 1a.<sup>29</sup> Based on prior work, it is known that DFAG-4T oligopeptides self-assemble into supramolecular 1-D fibers by lowering the solution pH,<sup>22</sup> typically by direct addition of acid or via vapor acid diffusion.<sup>22</sup> However, the direct addition of acid results in rapid, kinetically controlled assembly,<sup>22</sup> yielding a gel-like material containing fibers with random orientations<sup>24</sup> that are difficult to align postassembly. From this perspective, the processability of  $\pi$ -conjugated oligopeptide fibers generated using these methods could be hindered for further applications. To overcome this limitation, we hypothesized that oligopeptides might spontaneously self-assemble into fibers with controlled orientations via concentration-driven evaporative assembly inside templated features on a solid substrate.

To proceed, we began by studying the evaporative assembly of DFAG-4T on nontemplated solid substrates, which occurs due to an increase in peptide concentration during solvent evaporation of DFAG-4T solutions. We prepared solutions of DFAG-4T in several polar solvents (aprotic and protic) with relatively low boiling points (Table S1), followed by evaporation of these solutions on solid substrates. We found that common polar solvents such as methanol, ethanol, acetone,

isopropanol, and acetonitrile yield discrete supramolecular fibers of DFAG-4T upon evaporation (Figure 1). Interestingly, it is noteworthy that diethyl ether is a more volatile solvent compared to methanol and acetone (boiling point of 35 °C at atmospheric pressure and vapor pressure of 58.7 kPa); however, diethyl ether was not able to induce evaporative assembly of DFAG-4T into discrete supramolecular fibers (Table S1). We conjecture that the apparent low solubility of DFAG-4T in diethyl ether and ethyl acetate likely gives rise to the lack of assembly upon evaporation from these solvents. In addition, DFAG-4T was readily soluble in dioxane; however, evaporation from this solvent did not yield self-assembled fiber-like structures. These results suggest that the dipole moment of the polar solvent used for evaporative assembly likely plays a role in inducing oligopeptide self-assembly because the peptide residue interactions can be affected by solvent polarity.

Following evaporative assembly onto nontemplated solid surfaces, we studied the optical and structural properties of DFAG-4T fibers using confocal fluorescence microscopy, scanning electron microscopy, and atomic force microscopy (AFM). In particular, two-photon confocal microscopy was used to acquire local fluorescence emission spectra of assembled DFAG-4T fibers with high spatial resolution. DFAG-4T fibers exhibit a fluorescence emission peak around 570 nm following evaporative self-assembly using methanol, ethanol, acetone, isopropanol, and acetonitrile as solvents (Figures S1–S5), which is consistent with the fluorescence emission spectrum of DFAG-4T assembled using acid vapor diffusion or direct addition of acid.<sup>22</sup> These results suggest that DFAG-4T fibers assembled using evaporative assembly exhibit similar  $\pi$ - $\pi$  stacking interactions between quaterthiophene cores relative to acid-induced assembly.<sup>22,31,32</sup>

Scanning electron microscopy (SEM) was further used to characterize the structural properties of DFAG-4T fibers using the evaporative assembly method. SEM images of assembled DFAG-4T peptides show discrete fibers following evaporative

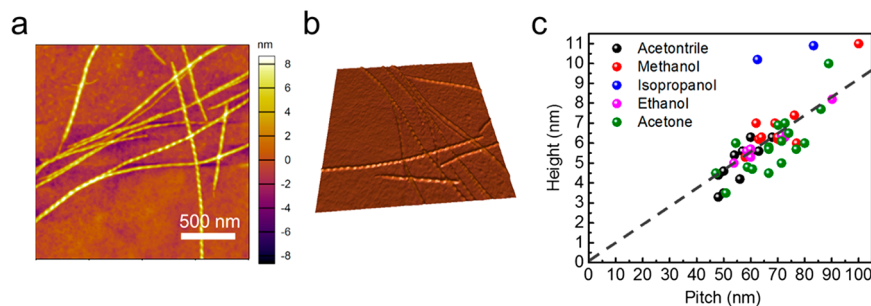


**Figure 2.** Atomic force microscopy (AFM) images of DFAG-4T oligopeptide fibers assembled using the evaporative assembly method on a solid surface. (a) 2-D and (b) 3-D AFM height images of DFAG-4T fibers assembled on a silicon wafer using methanol as solvent (image size  $2 \times 2 \mu\text{m}$ ). (c) Height and pitch relationship of helical DFAG-4T fibers using evaporative assembly in different organic solvents.

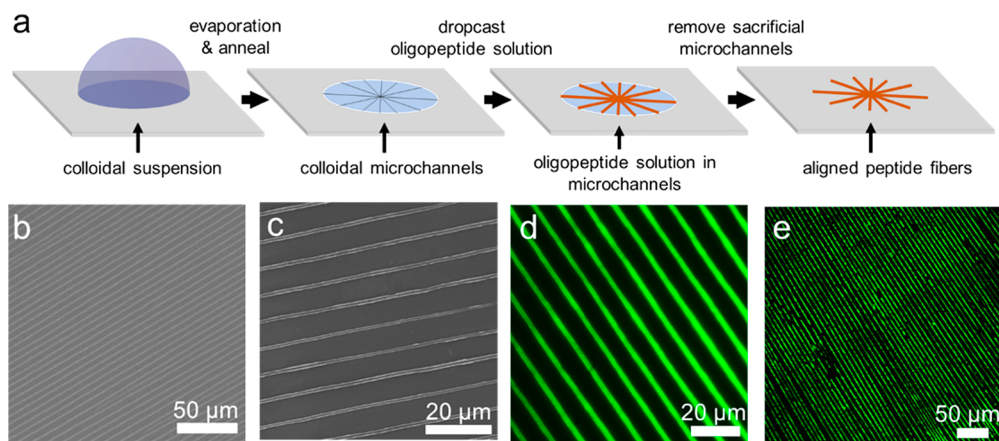


**Figure 3.** Assembly and alignment of  $\pi$ -conjugated oligopeptides using a colloidal microchannel templating method. (a) Schematic illustration of method to prepare colloidal microchannels, followed by evaporative assembly of oligopeptides and removal of sacrificial microchannels. (b) SEM image of highly ordered colloidal microchannels. (c) SEM image and (d,e) fluorescence emission images of aligned DFAG-4T fibers after removal of the sacrificial colloidal microchannel template.

assembly using methanol, ethanol, acetone, isopropanol, and acetonitrile (Figure 1b–f). However, a large amount of unassembled DFAG-4T peptide was detected in the fluorescence emission spectra using THF as a solvent for evaporative assembly, with some local areas showing a fluorescence emission peak around a wavelength of 500 nm (Figure S6), which is characteristic of unassembled DFAG-4T peptide. These results are consistent with SEM images of DFAG-4T following evaporation of THF, which show evidence of oligopeptide aggregation postassembly (Figure 1g). We further investigated the role of solution alkalinity in controlling assembly by adding a strong base (sodium hydroxide) to assembling solutions of DFAG-4T. We found that DFAG-4T assembles into robust supramolecular fibers even in the presence of 0.1 mM sodium hydroxide, comparable to pH  $\approx$  10 in aqueous solution (Figure S7).

We further characterized the structure of assembled oligopeptide fibers using AFM (Figures 2 and S8). Interestingly, these results show that DFAG-4T assembles into helical fibers by evaporative self-assembly, and the helical pitch of fibers is impacted by the selection of solvent for evaporative assembly. We found an approximately linear relationship between the pitch and height of assembled helical fibers, as shown in Figure 2. Prior work has reported the appearance of assembled  $\pi$ -conjugated oligopeptides with helical structures;<sup>28</sup> however, self-assembled fibers in prior studies were prepared by direct addition of acid rather than using evaporative self-assembly. Our results suggest that the nature of the organic

solvent ultimately affects the local molecular and supramolecular structure during evaporative assembly, specifically resulting in changes in the geometry (height and pitch) of assembled helices.

Following optical and structural characterization, we next used colloidal microchannels to generate large ordered arrays of assembled  $\pi$ -conjugated oligopeptides. In these experiments, evaporative assembly of DFAG-4T was performed on solid substrates containing highly ordered colloidal microchannels as templates for peptide assembly (Figure 3a). Colloidal microchannels are created by simply drying a colloidal suspension (1% w/w polystyrene latex nanoparticles, 47 nm diameter) on a silicon wafer at 55 °C, which results in the generation of a colloidal film containing ordered microchannels due to capillary stress gradients (Figure 3b).<sup>33</sup> Using this approach, colloidal microchannels were created over large areas ( $1 \times 1 \text{ cm}^2$ ) with channel widths on the order of  $\sim$ 500 nm and a regular periodic spacing of  $\sim$ 10  $\mu\text{m}$  between channels. Although colloidal microchannels are formed with a spoke-like orientation across the entire wafer (global area of  $\text{cm}^2$ ), the microchannels are locally parallel (local area of 100–500  $\mu\text{m}^2$ ) (Figure 3b). Following drying of the colloidal suspension, the prepared colloidal microchannel pattern was thermally annealed near the glass transition temperature of polystyrene ( $T_g = 105^\circ\text{C}$ ) for 30 min to remove local defects in the film. Importantly, we found that thermal annealing is essential in preparing colloidal microchannel films. In particular, SEM images of colloidal films before and after thermal annealing reveal a key morphology

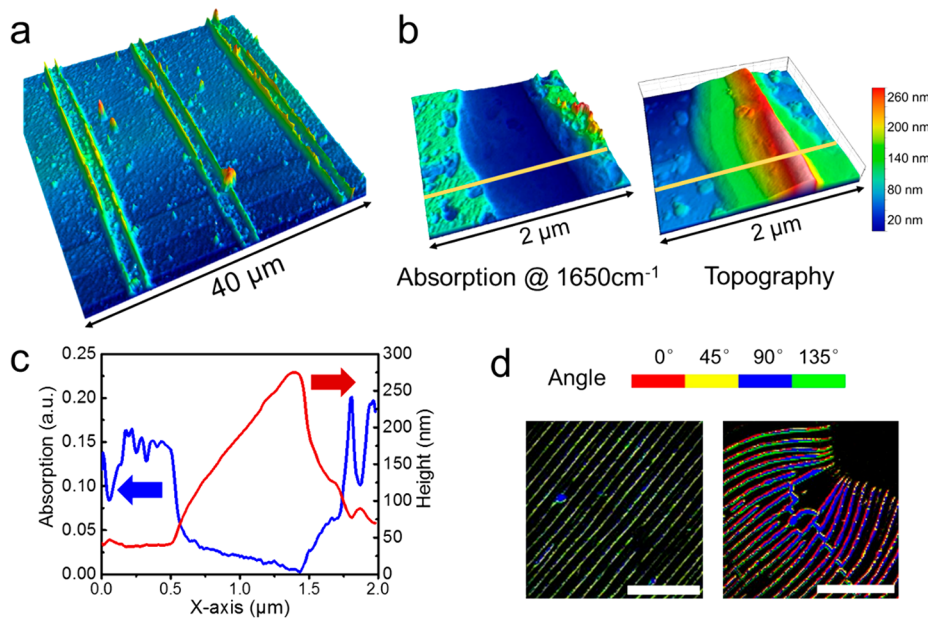


**Figure 4.** Atomic force microscope–infrared spectroscopy (AFM–IR) and AFM imaging of  $\pi$ -conjugated oligopeptides using the colloidal microchannel templating method. (a) AFM images of aligned DFAG-4T fibers. (b) Left: AFM–IR spectroscopy showing absorption at  $1650\text{ cm}^{-1}$  and right: surface topography image of a single DFAG-4T assembled structure. (c) AFM–IR absorption at  $1650\text{ cm}^{-1}$  and AFM height profiles of the yellow line in part (b). (d) Polarized fluorescence emission microscopy images of parallel and curved DFAG-4T features formed using the colloidal microchannel templating method. Color corresponds to fluorescence emission at different polarized angles. Scale bar =  $100\text{ }\mu\text{m}$ .

change in colloidal microchannels: before thermal annealing, multiple structural defects (particle vacancies) exist between closely packed PS latex particles (Figure S9a). However, particle vacancies are nearly fully removed after thermal annealing above  $T_g$  for 10 min (Figure S9b) and completely vanish after 20 min (Figure S9c,d). Thermal annealing converts a porous colloidal film into a smooth film containing discrete microchannels, which prevents the diffusion of peptide in the material between microchannels (Figure S10).

Following thermal annealing and preparation of colloidal microchannels, a solution of DFAG-4T peptide was drop cast near the center of the microchannel patterns, which allowed the DFAG-4T solution to flow through the channels via capillary forces. Following evaporative assembly, the sacrificial microchannel film was removed using a selective organic solvent (toluene) that preferentially dissolves polystyrene but is immiscible with DFAG-4T. Following removal of the sacrificial microchannels, a large array of DFAG-4T fibers with long-range ordering was obtained (Figure 3c). Two-photon fluorescence microscopy was used to characterize DFAG-4T fibers assembled using the microchannel templating method (Figure 3d,e), which revealed high degrees of alignment over relatively large areas. Taken together, these confocal and optical imaging experiments reveal that the assembled supramolecular fibers retain their structural and photophysical properties after removal of the sacrificial colloidal microchannels.

We used two scanning probe spectral imaging techniques, AFM–IR imaging and photoinduced force microscopy (PiFM), to characterize the chemical and structural properties of DFAG-4T fibers assembled using the microchannel templating method. AFM–IR provides the infrared absorbance spectrum for a material, together with surface topology, at high spatial resolution ( $\leq 10\text{ nm}$  resolution). PiFM, on the other hand, measures the local polarizability of the material at the nanoscale. Surprisingly, AFM measurements (Figure 4a) and AFM–IR absorption measurements on DFAG-4T fibers

aligned in colloidal microchannels revealed that these structures generally consist of two separate features, presumably corresponding to peptide aligned along the edges of the sacrificial microchannel walls. Our results show that the aligned and assembled oligopeptide structures are of order  $1\text{ }\mu\text{m}$  in width. Moreover, AFM images show that the height of deposited fibers is  $\sim 200\text{ nm}$ , indicating that these structures are likely composed of bundles of DFAG-4T fibers, given that the diameter of a single DFAG-4T fiber is  $\sim 6\text{ nm}$ , as shown in Figure 2c.

AFM–IR spectroscopy further provides additional information regarding the local structure of the flanking peptide sequence. AFM–IR measurements on individual DFAG-4T deposited structures show a strong IR absorption at wavelength of  $1650\text{ cm}^{-1}$  (Figure 4b), which can be attributed to the amide I absorption band in beta-sheet rich structures of assembled DFAG-4T fibers.<sup>34</sup> It is also worth noting that the tallest deposited feature of assembled DFAG-4T exhibited the maximum infrared absorption (Figure 4c), which is consistent with the surface topology. We further used polarized fluorescence emission microscopy to study the orientation of microchannel-assembled DFAG-4T fibers (Figure 4d). DFAG-4T peptide assembled into parallel lines showed similar polarized fluorescence emission features (Figure 4d, left panel). However, by intentionally selecting a microchannel defect area that has two sets of parallel DFAG-4T fibers meeting at a  $45^\circ$  angle, we found that the lower right set of parallel assembled lines exhibited strong fluorescence emission when polarized at  $90^\circ$  (blue color, Figure 4d, right panel), whereas the upper left set of parallel lines exhibited emission at  $135^\circ$  (green color, Figure 4d, right panel). Taken together, results from polarized fluorescence emission microscopy suggest that DFAG-4T fibers tend to be aligned along the direction of colloidal microchannels.

We further used PiFM to obtain a detailed, high-resolution view of oligopeptide alignment using the microchannel

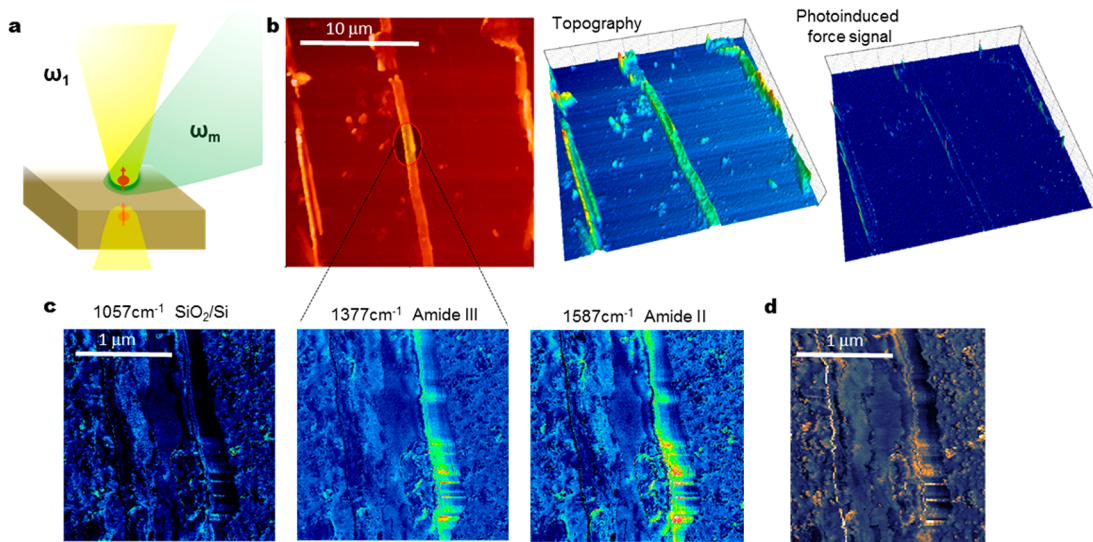


**Figure 5.** Photoinduced force microscopy (PiFM) of assembled and aligned oligopeptides. (a) Schematic of the experimental geometry of the PiFM setup. (b) 2-D and 3-D images of the topography of three microchannel-aligned DFAG-4T fibers (left and middle panel); PiFM response at 1600  $\text{cm}^{-1}$  (right panel). (c) Photoinduced spectral response of microchannel-aligned DFAG-4T fibers at three discrete wavelengths, 1057  $\text{cm}^{-1}$  (substrate response), 1377  $\text{cm}^{-1}$ , and 1587  $\text{cm}^{-1}$ . (d) Integrated hyperspectral image of photoinduced spectral response, where the integrated spectral intensity (from 780 to 1930  $\text{cm}^{-1}$ ) at each image pixel is shown.

templating approach. As previously noted, PiFM measures the local polarizability of a material at the excitation wavelength. In this way, PiFM offers interesting insights into the structural details of a material. Figure 5a shows a schematic of the experimental geometry.<sup>35,36</sup> The key feature for the PiFM experimental setup lies in realizing that the optical excitation polarizes the material in the sample volume, which in turn generates an image dipole in the tip of the cantilever. This local dipole–dipole interaction ultimately gives rise to a very weak photoinduced force, which is detected via resonant coupling to the higher order mechanical modes of the cantilever. In this work, we operate PiFM in hyperspectral mode by measuring the PiFM response across the IR window as a function of spatial position. Unlike AFM–IR, which measures integrated absorption of the species of interest, PiFM is more influenced by local polar order, which is illustrated in Figure 5b–d. Figure 5b (left and middle panel) shows the topography of three microchannel-aligned structures, and the right panel in Figure 5b shows the PiFM response at 1600  $\text{cm}^{-1}$ . In these images, the enhanced polarization is clearly observed at the structure edges. This effect is more dramatically illustrated in Figure 5c,d, where the photoinduced spectral response is shown. In particular, Figure 5c shows three discrete wavelengths: 1057  $\text{cm}^{-1}$  (substrate response), 1377  $\text{cm}^{-1}$  (amide III), and 1587  $\text{cm}^{-1}$  (amide II). Figure 5d shows the integrated hyperspectral image, where the integrated spectral intensity (from 780 to 1930  $\text{cm}^{-1}$ ) at each image pixel is shown. Again, the enhanced polar response at the structure edges is apparent. Finally, the full deconstructed hyperspectral image is shown in Figure S11.

In an additional set of experiments, we prepared two-dimensional (2-D) web-like colloidal microchannels via evaporation of polystyrene latex nanoparticle suspensions on a glass substrate rather than a silicon wafer. We hypothesize that differences in the thermal expansion coefficients of these different substrates lead to differences in lateral stresses during drying, resulting in either 1-D or 2-D colloidal microchannel arrays. In any case, we studied the evaporative assembly of DFAG-4T in 2-D web-like colloidal microchannels (Figure

S12). Our results show that the fluorescence emission properties of DFAG-4T fibers in 2-D channels is in general agreement with the assembled peptide materials generated in long linear arrays of ordered microchannels.

The charge transport properties of assembled DFAG-4T were further characterized using interdigitated electrodes and conductive AFM (Figure 6). In the first approach, we deposited DFAG-4T fibers onto interdigitated array (IDA) electrodes with 2  $\mu\text{m}$  channel length using evaporative assembly in methanol. Following fiber deposition, we measured the current–voltage ( $I$ – $V$ ) response in a two-point-probe geometry (Figure 6a). Nonlinear  $I$ – $V$  curves were obtained by sweeping the applied bias from –10 to 10 V. The overall structures of these  $I$ – $V$  curves are reminiscent of semiconductor junctions,<sup>37</sup> which can be rationalized by considering the Schottky barriers.<sup>38</sup> Moreover, a hysteresis loop in  $I$ – $V$  curves was observed in these measurements, though this could arise due to several effects<sup>39</sup> such as interfacial charge traps. Notably, the conductivity of DFAG-4T fibers was observed to be stable across multiple voltage sweep trials, such that the conductivity of DFAG-4T fibers remained unchanged during multiple cycles of applied bias between –10 to 10 V. However, when the applied voltage was increased above 40 V, repeated  $I$ – $V$  measurements resulted in a continuous decrease in conductivity (Figure S13). These results indicate that self-assembled DFAG-4T fibers are not stable under high applied bias, which may be attributed to joule heating that could jeopardize the self-assembled oligopeptide fibers. After scanning the  $I$ – $V$  curve across a high voltage range (100 V), the conductivity of DFAG-4T fibers reduced and could not be recovered under repeated measurements of sweeping the bias between –10 and 10 V (Figure 6a).

In addition to conductivity measurement along the fibers, we also used conductive AFM to measure the transverse conductivity of assembled DFAG-4T (Figures 6b and S13). First, we deposited DFAG-4T fibers on a gold substrate using evaporative assembly in methanol. In general, conductive AFM measurements generally showed that DFAG-4T fibers exhibited

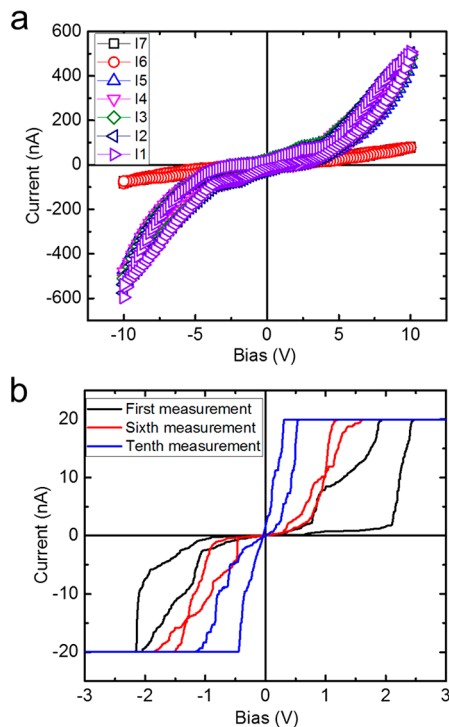


**Figure 6.** Electrical properties and conductance of assembled DFAG-4T. (a) Current–voltage ( $I$ – $V$ ) measurements of DFAG-4T using interdigitated array (IDA) electrodes. The bias was ramped from  $-10$  to  $10$  V over multiple iterations (11–15) before and after applying  $100$  V (16–17). After application of high voltage, the  $I$ – $V$  curves show a dramatic change, suggesting structural rearrangements under high bias. (b) Single-point conductivity measurements of DFAG-4T fibers using conductive AFM.

a lower conductivity compared to a clean gold substrate (Figure S14), which is expected because the peptide flanking sequence DFAG has a much higher resistance compared to gold, and quaterthiophene (4T) is known to be a p-type organic semiconductor. We also performed single-point conductivity measurements using an AFM tip (denoted with an asterisk in Figure S14). Interestingly, repeated measurements of lateral conductivity of DFAG-4T resulted in enhanced conductance. We conjecture that the enhanced conductivity could occur due to peptide fiber orientation and alignment in the presence of a strong electric field used for conductive AFM over repeated measurements on the same sample area or AFM-tip-induced electrochemical reduction along the DFAG-4T fiber backbone.<sup>40</sup>

## CONCLUSIONS

In this work, we demonstrate that evaporation of a polar solvent containing  $\pi$ -conjugated oligopeptide effectively induces molecular self-assembly into ordered supramolecular structures. Interestingly, the helicity of assembled single DFAG-4T fibers is affected by the nature of the organic solvent used for evaporative self-assembly. Evaporative assembly was effectively combined with a colloidal microchannel templating method, thereby generating highly aligned DFAG-4T fibers over large areas, which were characterized by fluorescence polarization microscopy to reveal high degrees of directional alignment.

Importantly, two scanning probe spectral imaging techniques, AFM–IR and PiFM, are utilized to characterize the

structural properties of assembled DFAG-4T fibers. Results from AFM–IR show a strong IR absorption at wavelength of  $1650\text{ cm}^{-1}$  for the assembled DFAG-4T fibers, indicating amide I absorption band in beta-sheet rich structures, while the PiFM response at  $1600\text{ cm}^{-1}$  shows clearly enhanced polarization at the structure edges. These scanning probe spectral imaging techniques (AFM–IR and PiFM) provide important insights into the detailed structural properties of aligned oligopeptide fibers, and these methods can be further utilized for characterizing other self-assembled nanomaterial systems. From a broad perspective, the colloidal microchannel templating strategy provides a simple yet robust method to macroscopically pattern 1-D assembled functional materials into well-ordered arrays, which could aid solution-based processing of soft organic electronic materials.

## ASSOCIATED CONTENT

### Supporting Information

The Supporting Information is available free of charge on the ACS Publications website at DOI: [10.1021/acsmami.7b13978](https://doi.org/10.1021/acsmami.7b13978).

Summary of experimental conditions for evaporative assembly; fluorescence imaging of DFAG-4T fibers using a variety of organic solvents; SEM and AFM images of assembled oligopeptide fibers; SEM images of colloidal films and microchannels; charge transport properties of DFAG-4T materials (PDF)

## AUTHOR INFORMATION

### Corresponding Author

\*E-mail: [cms@illinois.edu](mailto:cms@illinois.edu) (C.M.S.)

### ORCID

Ying Diao: [0000-0002-8984-0051](https://orcid.org/0000-0002-8984-0051)

Charles M. Schroeder: [0000-0001-6023-2274](https://orcid.org/0000-0001-6023-2274)

### Notes

The authors declare no competing financial interest.

## ACKNOWLEDGMENTS

We thank Herdeline Ann M. Ardoña and John D. Tovar for providing the  $\pi$ -conjugated synthetic oligopeptides, the staff and resources at the Frederick Seitz Materials Research Laboratory for facilities and instrumentation, and Dr. Antonio Ambrosio and the scanning probe instrumental resources at the Center for Nanoscale Systems at Harvard University. In addition, we thank the teams at Molecular Vista and Block Engineering for the loan of a fast tuning QCL (LaserTune), which enabled the hyperspectral PiFM work. This work was supported by the U.S. Department of Energy, Office of Science, Basic Energy Sciences (BES) under Award #SC-0011847.

## REFERENCES

- (1) Aida, T.; Meijer, E. W.; Stupp, S. I. Functional Supramolecular Polymers. *Science* **2012**, *335*, 813–817.
- (2) Henson, Z. B.; Mullen, K.; Bazan, G. C. Design strategies for organic semiconductors beyond the molecular formula. *Nat. Chem.* **2012**, *4*, 699–704.
- (3) Faramarzi, V.; Niess, F.; Moulin, E.; Maaloum, M.; Dayen, J.-F.; Beaufrand, J.-B.; Zanettini, S.; Doudin, B.; Giuseppone, N. Light-triggered self-construction of supramolecular organic nanowires as metallic interconnects. *Nat. Chem.* **2012**, *4*, 485–490.
- (4) Oh, J. H.; Lee, H. W.; Mannsfeld, S.; Stoltberg, R. M.; Jung, E.; Jin, Y. W.; Kim, J. M.; Yoo, J.-B.; Bao, Z. Solution-processed, high-

- performance n-channel organic microwire transistors. *Proc. Natl. Acad. Sci. U. S. A.* **2009**, *106*, 6065–6070.
- (5) Hong, J.-P.; Um, M.-C.; Nam, S.-R.; Hong, J.-I.; Lee, S. Organic single-nanofiber transistors from organogels. *Chem. Commun.* **2009**, 310–312.
- (6) Giansante, C.; Raffy, G.; Schäfer, C.; Rahma, H.; Kao, M.-T.; Olive, A. G. L.; Del Guerzo, A. White-Light-Emitting Self-Assembled NanoFibers and Their Evidence by Microspectroscopy of Individual Objects. *J. Am. Chem. Soc.* **2011**, *133*, 316–325.
- (7) Kwiat, M.; Cohen, S.; Pevzner, A.; Patolsky, F. Large-scale ordered 1D-nanomaterials arrays: Assembly or not? *Nano Today* **2013**, *8*, 677–694.
- (8) Iijima, S.; Ichihashi, T. Single-shell carbon nanotubes of 1-nm diameter. *Nature* **1993**, *363*, 603–605.
- (9) Tans, S. J.; Verschueren, A. R. M.; Dekker, C. Room-temperature transistor based on a single carbon nanotube. *Nature* **1998**, *393*, 49–52.
- (10) Yu, G.; Cao, A.; Lieber, C. M. Large-area blown bubble films of aligned nanowires and carbon nanotubes. *Nat. Nanotechnol.* **2007**, *2*, 372–377.
- (11) Yao, J.; Yan, H.; Lieber, C. M. A nanoscale combing technique for the large-scale assembly of highly aligned nanowires. *Nat. Nanotechnol.* **2013**, *8*, 329–335.
- (12) Cao, Q.; Han, S.-j.; Tulevski, G. S.; Zhu, Y.; Lu, D. D.; Haensch, W. Arrays of single-walled carbon nanotubes with full surface coverage for high-performance electronics. *Nat. Nanotechnol.* **2013**, *8*, 180–186.
- (13) He, X.; Gao, W.; Xie, L.; Li, B.; Zhang, Q.; Lei, S.; Robinson, J. M.; Hároz, E. H.; Doorn, S. K.; Wang, W.; Vajtai, R.; Ajayan, P. M.; Adams, W. W.; Hauge, R. H.; Kono, J. Wafer-scale monodomain films of spontaneously aligned single-walled carbon nanotubes. *Nat. Nanotechnol.* **2016**, *11*, 633–638.
- (14) Cao, Q.; Tersoff, J.; Farmer, D. B.; Zhu, Y.; Han, S.-J. Carbon nanotube transistors scaled to a 40-nanometer footprint. *Science* **2017**, *356*, 1369–1372.
- (15) He, M.; Zhao, L.; Wang, J.; Han, W.; Yang, Y.; Qiu, F.; Lin, Z. Self-Assembly of All-Conjugated Poly(3-alkylthiophene) Diblock Copolymer Nanostructures from Mixed Selective Solvents. *ACS Nano* **2010**, *4*, 3241–3247.
- (16) He, M.; Ge, J.; Fang, M.; Qiu, F.; Yang, Y. Fabricating polythiophene into highly aligned microwire film by fast evaporation of its whisker solution. *Polymer* **2010**, *51*, 2236–2243.
- (17) Byun, M.; Laskowski, R. L.; He, M.; Qiu, F.; Jeffries-El, M.; Lin, Z. Controlled evaporative self-assembly of hierarchically structured regioregular conjugated polymers. *Soft Matter* **2009**, *5*, 1583–1586.
- (18) Ardoña, H. A. M.; Tovar, J. D. Peptide π-Electron Conjugates: Organic Electronics for Biology? *Bioconjugate Chem.* **2015**, *26*, 2290–2302.
- (19) Hartgerink, J. D.; Beniash, E.; Stupp, S. I. Peptide-amphiphilic nanofibers: A versatile scaffold for the preparation of self-assembling materials. *Proc. Natl. Acad. Sci. U. S. A.* **2002**, *99*, 5133–5138.
- (20) Stupp, S. I.; Palmer, L. C. Supramolecular Chemistry and Self-Assembly in Organic Materials Design. *Chem. Mater.* **2014**, *26*, 507–518.
- (21) Xu, X.-D.; Lin, B.-B.; Feng, J.; Wang, Y.; Cheng, S.-X.; Zhang, X.-Z.; Zhuo, R.-X. Biological Glucose Metabolism Regulated Peptide Self-Assembly as a Simple Visual Biosensor for Glucose Detection. *Macromol. Rapid Commun.* **2012**, *33*, 426–431.
- (22) Li, B.; Li, S.; Zhou, Y.; Ardoña, H. A. M.; Valverde, L. R.; Wilson, W. L.; Tovar, J. D.; Schroeder, C. M. Nonequilibrium Self-Assembly of π-Conjugated Oligopeptides in Solution. *ACS Appl. Mater. Interfaces* **2017**, *9*, 3977–3984.
- (23) Ardoña, H. A. M.; Draper, E. R.; Citossi, F.; Wallace, M.; Serpell, L. C.; Adams, D. J.; Tovar, J. D. Kinetically Controlled Coassembly of Multichromophoric Peptide Hydrogelators and the Impacts on Energy Transport. *J. Am. Chem. Soc.* **2017**, *139*, 8685–8692.
- (24) Zhou, Y.; Li, B.; Li, S.; Ardoña, H. A. M.; Wilson, W. L.; Tovar, J. D.; Schroeder, C. M. Concentration-Driven Assembly and Sol–Gel Transition of π-Conjugated Oligopeptides. *ACS Cent. Sci.* **2017**, *3*, 986–994.
- (25) Brunsved, L.; Folmer, B. J. B.; Meijer, E. W.; Sijbesma, R. P. Supramolecular Polymers. *Chem. Rev.* **2001**, *101*, 4071–4098.
- (26) Velichko, Y. S.; Stupp, S. I.; de la Cruz, M. O. Molecular Simulation Study of Peptide Amphiphile Self-Assembly. *J. Phys. Chem. B* **2008**, *112*, 2326–2334.
- (27) Li, B.; Jiang, B.; Han, W.; He, M.; Li, X.; Wang, W.; Hong, S. W.; Byun, M.; Lin, S.; Lin, Z. Harnessing Colloidal Crack Formation by Flow-Enabled Self-Assembly. *Angew. Chem., Int. Ed.* **2017**, *56*, 4554–4559.
- (28) Diegelmann, S. R.; Gorham, J. M.; Tovar, J. D. One-Dimensional Optoelectronic Nanostructures Derived from the Aqueous Self-Assembly of π-Conjugated Oligopeptides. *J. Am. Chem. Soc.* **2008**, *130*, 13840–13841.
- (29) Vadehra, G. S.; Wall, B. D.; Diegelmann, S. R.; Tovar, J. D. On-resin dimerization incorporates a diverse array of [small pi]-conjugated functionality within aqueous self-assembling peptide backbones. *Chem. Commun.* **2010**, *46*, 3947–3949.
- (30) Han, W.; Li, B.; Lin, Z. Drying-Mediated Assembly of Colloidal Nanoparticles into Large-Scale Microchannels. *ACS Nano* **2013**, *7*, 6079–6085.
- (31) Hestand, N. J.; Spano, F. C. Molecular Aggregate Photophysics beyond the Kasha Model: Novel Design Principles for Organic Materials. *Acc. Chem. Res.* **2017**, *50*, 341–350.
- (32) Spano, F. C.; Yamagata, H. Vibronic Coupling in J-Aggregates and Beyond: A Direct Means of Determining the Exciton Coherence Length from the Photoluminescence Spectrum. *J. Phys. Chem. B* **2011**, *115*, 5133–5143.
- (33) Allain, C.; Limat, L. Regular Patterns of Cracks Formed by Directional Drying of a Colloidal Suspension. *Phys. Rev. Lett.* **1995**, *74*, 2981–2984.
- (34) Webster, G. T.; Dusting, J.; Balabani, S.; Blanch, E. W. Detecting the Early Onset of Shear-Induced Fibril Formation of Insulin in situ. *J. Phys. Chem. B* **2011**, *115*, 2617–2626.
- (35) Jahng, J.; Fishman, D. A.; Park, S.; Nowak, D. B.; Morrison, W. A.; Wickramasinghe, H. K.; Potma, E. O. Linear and Nonlinear Optical Spectroscopy at the Nanoscale with Photoinduced Force Microscopy. *Acc. Chem. Res.* **2015**, *48*, 2671–2679.
- (36) Nowak, D.; Morrison, W.; Wickramasinghe, H. K.; Jahng, J.; Potma, E.; Wan, L.; Ruiz, R.; Albrecht, T. R.; Schmidt, K.; Frommer, J.; Sanders, D. P.; Park, S. Nanoscale chemical imaging by photoinduced force microscopy. *Science Advances* **2016**, *2*, e1501571.
- (37) Zhang, Z.; Yao, K.; Liu, Y.; Jin, C.; Liang, X.; Chen, Q.; Peng, L. M. Quantitative Analysis of Current–Voltage Characteristics of Semiconducting Nanowires: Decoupling of Contact Effects. *Adv. Funct. Mater.* **2007**, *17*, 2478–2489.
- (38) Valencia, D.; Whiting, G. T.; Bulo, R. E.; Weckhuysen, B. M. Protonated thiophene-based oligomers as formed within zeolites: understanding their electron delocalization and aromaticity. *Phys. Chem. Chem. Phys.* **2016**, *18*, 2080–2086.
- (39) Müller, R.; Naulaerts, R.; Billen, J.; Genoe, J.; Heremans, P. CuTCNQ resistive nonvolatile memories with a noble metal bottom electrode. *Appl. Phys. Lett.* **2007**, *90*, 063503.
- (40) Mativetsky, J. M.; Treossi, E.; Orgiu, E.; Melucci, M.; Veronese, G. P.; Samori, P.; Palermo, V. Local Current Mapping and Patterning of Reduced Graphene Oxide. *J. Am. Chem. Soc.* **2010**, *132*, 14130–14136.